THE JOURNAL OF PHYSICAL CHEMISTRY B

Article

pubs.acs.org/JPCB

# Amphiphile Micelle Structures in the Protic Ionic Liquid Ethylammonium Nitrate and Water

Zhengfei Chen,[†,‡] Tamar L. Greaves,[‡,§] Rachel A. Caruso,*[,†,‡] and Calum J. Drummond*[,‡,§]

[†]Particulate Fluids Processing Centre (PFPC), School of Chemistry, The University of Melbourne, Melbourne, Victoria 3010, Australia

[‡]CSIRO Materials Science and Engineering, Bag 10, Clayton South MDC, Victoria 3169, Australia

[§]School of Applied Sciences, College of Science, Engineering and Health, RMIT University, GPO Box 2476, Melbourne, Victoria 3001, Australia

Supporting Information

**ABSTRACT:** Micelles formed by amphiphiles in a protic ionic liquid (PIL), ethylammonium nitrate (EAN), were investigated using synchrotron small-angle X-ray scattering and contrasted with those that formed in water. The amphiphiles studied were cationic hexadecyltrimethylammonium chloride (CTAC) and hexadecylpyridinium bromide (HDPB) and nonionic poly(oxyethylene) (10) oleyl ether (Brij 97) and Pluronic ethylene oxide−propylene oxide−ethylene oxide block copolymer (P123). The scattering patterns were analyzed using spherical, core−shell, and cylindrical scattering models. The apparent micelle shape and size of the surfactants and the block copolymer in the PIL have been reported. At low amphiphile concentrations (<10 wt %) spherical micelles were preferentially formed for all the amphiphiles in EAN. The micelles formed by the two cationic amphiphiles in EAN and water were similar, though different scattering models were required predominantly due to the ionic nature of EAN. The two nonionic amphiphiles formed micelles with similar core radii in water and in EAN. However, the micelle shells composed of ethylene oxide groups fitted to a significantly thicker layer in water compared to EAN. At high concentrations (>10 wt %) in EAN and water, there was a preference for cylindrical micelles for CTAC, HDPB, and Brij 97; however, the P123 micelles remained spherical.

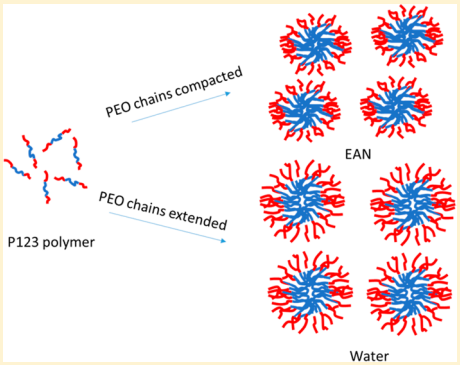


## INTRODUCTION

The ability of amphiphiles to form micelles and lyotropic liquid crystal phases is governed by the solvophobic effect in nonaqueous solvents, analogous to the hydrophobic effect in water.[1] The vast majority of the literature on amphiphile self-assembly has involved the investigation of extensive libraries of amphiphiles in water and with the addition of salts and cosurfactants.[2] Protic ionic liquids (PILs), which are produced through a stoichiometric combination of a Brønsted acid and a Brønsted base,[3] can be considered as the most tailorable class of solvents that have a widespread ability to support amphiphile self-assembly.[3−6] The solvophobic effect of many PILs is attributed to their high cohesive energy density, in part due to their ability to form 3-D hydrogen-bonded networks, similar to water.[1,3] The micellization process and lyotropic liquid crystalline structures at higher amphiphile concentrations are highly dependent on the specific solvent and amphiphile combination.[1−4] For some amphiphiles, micelles are formed above the critical micelle concentration (cmc) at appropriate temperatures (above the Kraft temperature), and the cmc varies considerably depending on the solvent and amphiphile combination.

The formation of micelles in protic and aprotic ionic liquids has only been reported for a few anionic amphiphiles, with studies focusing predominantly on cationic amphiphiles.[3,4,7,8] To the best of our knowledge, the micelle formation of nonionic amphiphiles in PILs has only included Triton X-100,[9] aerosol OT (AOT),[10] alkyl oligo(ethylene oxide)s ($C_nE_m$),[11−13] and phytosterol ethoxylate.[14] The cmc for various cationic[15] and nonionic amphiphiles[11,12] in PILs has been determined using light scattering or surface tension techniques. However, obtaining information about the micelle structure is more difficult. Direct visualization of micelles by cryo transmission electron microscopy (cryo-TEM) has been employed,[16] but this process is time-consuming, expensive, and relatively difficult for micelles in solvents other than water. Scattering techniques, such as small-angle X-ray scattering (SAXS) or small-angle neutron scattering (SANS), have been widely used for analyzing the size and structure of micelles. It is not possible to directly obtain information from the scattering patterns, since the scattering patterns from micelles are not associated with characteristic sharp peaks, such as are seen for lyotropic liquid crystalline phases in the scattering patterns. Instead, the SANS/SAXS patterns need to be fitted using a suitable

Received: September 22, 2014
Revised: November 29, 2014
Published: December 9, 2014





DOI: 10.1021/jp509557z
J. Phys. Chem. B 2015, 119, 179−191

scattering model.[17−24] Only two investigations have been reported on the small-angle scattering from the micelles of nonionic amphiphiles using neutrons[11] or X-rays,[12] and we are not aware of any such studies using cationic amphiphiles in ionic liquids.

A series of nonionic surfactants ($C_nE_m$) in ethylammonium nitrate (EAN) were shown by using SAXS to most likely form ellipsoid micelles.[12] In this case, only the micelle cores were fitted due to the low electron density contrast between the headgroups and EAN. However, core−shell ellipses for the micelles formed by $C_nE_m$ in EAN were reported using SANS with a polydispersity model.[11] Although the shell was fitted by this method, the shell thickness of the micelles could still be underestimated due to the poor contrast. The nonionic surfactants had much higher cmc values in aprotic ionic liquids than in water, and the micelle size was smaller in ionic liquids compared to water.[25,26] Cationic surfactants have been studied by Evans et al. in EAN and compared to those in water; the cmcs in EAN were much higher than in water.[15,27] These findings clearly show that the micelles formed in ionic liquids can be different from those formed in water.

The packing of amphiphile molecules in solvents is determined by the competing interactions of the polar headgroups and alkyl chains whereby the shape factor or critical packing parameter (CPP) is defined as

$$\mathrm{CPP} = v/al_c \quad (1)$$

where $l_c$ is the effective length of the amphiphile chain, $a$ is the effective amphiphile headgroup area, and $v$ is the average volume occupied by an amphiphile molecule.[28] Spherical micelles form for CPP less than or equal to 1/3, rodlike micelles form for a CPP between 1/3 and 1/2, and bilayers form for CPP values between 1/2 and 1. The nature of the solvent influences the size and structure of the micelles,[21,29] giving rise to different micelle properties in various PILs, water, and molecular solvents.[4,5,30] The shapes of micelles formed by amphiphiles at low concentrations (but above the cmc) in aqueous and some nonaqueous solvents range from globular (spheres and ellipsoids)[31] to rodlike (cylinders and wormlike)[16] or bilayers (disks).[32] When amphiphiles are effectively "wedge-shaped" (CPP $\leq$ 1/3), spherical micelles are thermodynamically favored over other shapes such as cylindrical micelles or bilayers.[28] Once aggregation numbers (number of amphiphiles in the micelles) exceed a certain limit, it is no longer possible to pack amphiphiles into spheres. This leads to the elongation of the micelles to form ellipsoids or rods. The addition of ions into solvents can screen the headgroup charge of charged amphiphiles, which may lead to an increase in the aggregation number and may result in a transition from sphere- to rod-shaped micelles.[33]

In the aqueous system, the phase sequence as a function of increasing surfactant concentration generally follows the trend of micellar, hexagonal, cubic, and lamellar lyotropic liquid crystalline phases.[34] The same sequence is observed in PILs, though often with less phase diversity.[3,5,35,36] Due to the ionic nature of PILs, the interactions with surfactants are more complex, particularly ionic surfactants, and PILs that contain alkyl chains are expected to behave to some extent as cosurfactants as the nonpolar alkyl domains interact with the surfactants.[27,37,38] Previously we have reported the lyotropic liquid crystalline phases formed by cationic hexadecyltrimethylammonium chloride (CTAC) and hexadecylpyridinium bromide (HDPB) and nonionic poly(oxyethylene) (10) oleyl ether (Brij 97) and Pluronic ethylene oxide−propylene oxide−ethylene oxide block copolymer (P123) in three PILs, as well as in water for comparison.[30] The three PILs used were EAN, ethanolammonium nitrate (EOAN), and diethanolammonium formate (DEOAF). The lyotropic liquid crystal phases present and their thermal stability ranges depended on the specific solvent−amphiphile combinations. In general, the lyotropic liquid crystal phases were only observed at amphiphile concentrations above 40 wt %. In the present work we explore the lower concentration region where micelles are formed by these amphiphiles in EAN, as well as in water for comparison.

In this paper we extend the understanding of micelle formation in EAN to include two cationic surfactants, one nonionic surfactant, and one nonionic block copolymer. The specific amphiphiles used were CTAC, HDPB, Brij 97 (a $C_{18}$ ethylene oxide surfactant), and a Pluronic P123 block copolymer (a poly(ethylene oxide) (PEO)−poly(propylene oxide) (PPO)−poly(ethylene oxide) copolymer). These micellar systems were characterized using SAXS with a powerful synchrotron light source since the contrast between the amphiphiles and solvents is very weak. To the best of our knowledge, this is the first report of small-angle scattering data for micelles formed from cationic or block copolymer amphiphiles in a PIL.

## EXPERIMENTAL SECTION

**Chemicals.** All chemicals were used as received. The four amphiphiles used were CTAC (Kodak), HDPB (Aldrich), Brij 97 ($CH_3(CH_2)_{17}(OCH_2CH_2)_nOH$, $n \approx 10$) (Aldrich), and a Pluronic block copolymer (PEO−PPO−PEO, $(EO)_{20}(PO)_{70}(EO)_{20}$, P123) (BASF). EAN was prepared according to the literature,[39] dried under rotary evaporation, and then further dried in a freeze-dryer overnight. The water content for EAN was determined as 0.48 wt % by Karl Fischer titration.

**SAXS Sample Preparation.** A series of concentrations (1, 3, 5, 10, and 20 wt %) for each of the four amphiphiles in EAN and in water were prepared. All samples at 1, 3, and 5 wt % were in the liquid state, and portions were transferred into 1 mm capillary tubes and sealed by wax to avoid solvent evaporation or water absorption in the use of EAN. Most samples at 10 and 20 wt % were very viscous, and portions were transferred to a purpose-built multiwell plate and sealed by Kapton tape. All samples were analyzed at the SAXS/WAXS beamline at the Australian Synchrotron. SAXS measurements covered the scattering vector range of $0.02 < q < 0.65$ Å$^{-1}$. The cationic surfactant samples were heated in a multiwell sample holder from 25 to 45 °C in 5 °C increments. An exposure time of 2 s was used for each sample at each temperature. The 2-D scattering patterns for SAXS were converted into 1-D scattering curves using SAXS 15-id software provided at the Australian Synchrotron. An empty capillary and empty well in the plate were used to obtain background scattering curves under the appropriate SAXS conditions, and these were subtracted from the sample scattering patterns. The SAXS patterns were fitted using a variety of scattering models in SansView to determine the most suitable model.

**Micelle Scattering Models.** The scattering intensity in the SAXS patterns for the micelles can be expressed by eq 2, where $I(q)$ is the scattering intensity, $K$ is a constant, $N$ is the number of scatterers, $P(q)$ is the form factor, and $S(q)$ is the structure factor.[17] The form factor describes the shape of the micelles,


DOI: 10.1021/jp509557z
J. Phys. Chem. B 2015, 119, 179−191

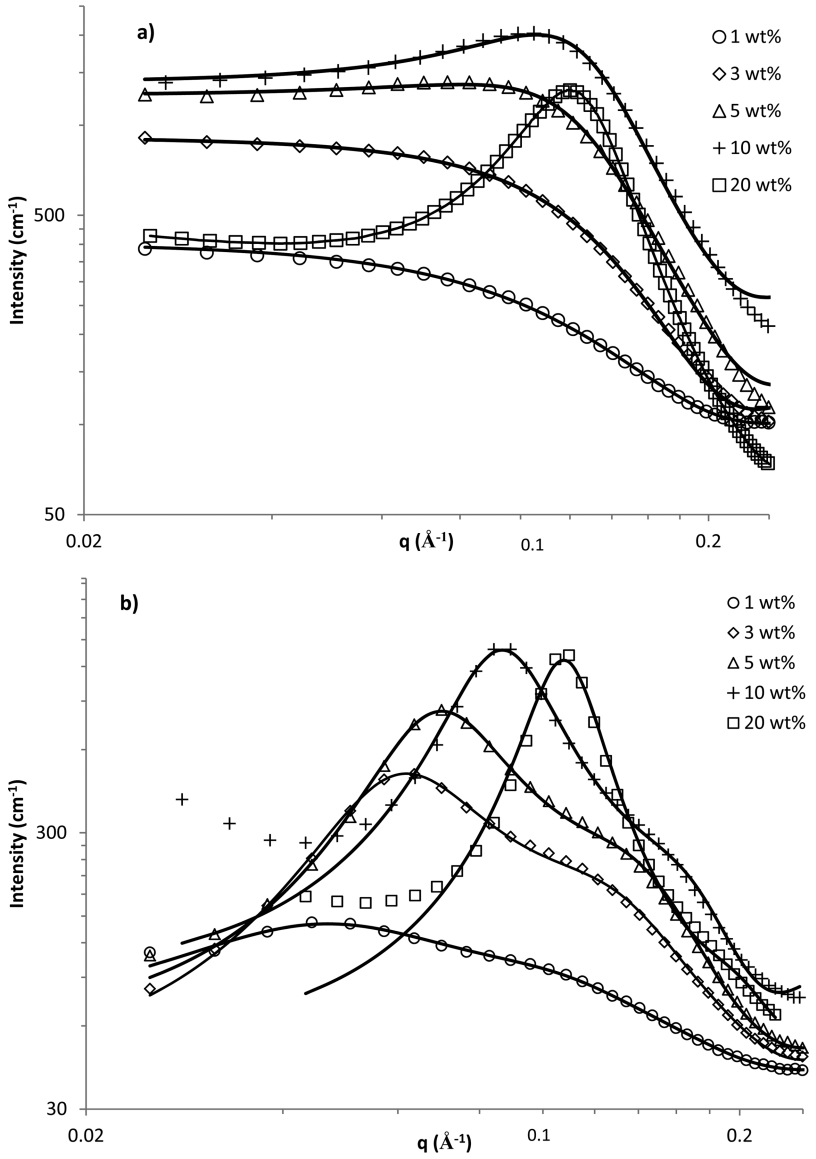


**Figure 1.** SAXS patterns for CTAC concentrations of 1, 3, 5, 10, and 20 wt % in (a) EAN and (b) water at 45 °C. The solid lines show the fits to the data.

such as spherical, core−shell, or cylindrical, and the structure factor describes the interactions between micelles.

$$I(q) = KN\ P(q)\ S(q) \quad (2)$$

In dilute solutions, micelle interactions can be neglected and the form factor alone describes the scattered intensity (the structure factor is effectively 1), so the $S(q)$ term can be removed from eq 2. However, the structure factor that describes interparticle (micelle) interactions needs to be included at relatively high concentrations. A comprehensive overview on modeling SAXS or SANS patterns is given by Pedersen, which includes the form factors for many micellar shapes and a variety of structure factors.[17] In this work, the spherical model (solid sphere or core−shell sphere) fitted the SAXS data best for low amphiphile concentrations (below 5 wt %), while a cylindrical model fitted well for high concentrations (10 and 20 wt %) for some systems. The scattering models used to fit the SAXS data were the sphere model, core−shell sphere model, cylinder model, and core−shell cylinder model (see the Supporting Information). To fit the data, we assume the cores (hydrocarbon or PPO) were not solvated; hence, the scattering length densities (SLDs) of the cores are fixed. The solvophilic headgroups were mixed with solvents, forming a shell for the amphiphiles containing large EO groups (Brij 97 and P123); therefore, a core−shell structure is used, and the SLD of the shell is fitted. However, we do not use a core−shell structure for the cationic surfactants as is discussed in the electron densities section.

**Electron Densities of Amphiphiles and Solvents.** For SAXS, the origin of the contrast contributing to the scattering is the difference in electron density between the micelles (particles) and the surrounding medium (solvent). The contrast can be different within the micelles, e.g., between the shell and the core, which gives high structural information contrast in the scattering pattern. The electron density can be estimated by $\rho_e^- = Z/V$, where $Z$ is the number of electrons and $V$ is the volume of the molecule. In fact, the SLD used in the modeling is directly related to its electron density, $\rho_e^-$, as SLD = $\rho_e^- r_e$, where $r_e$ is the electron radius. The volume and electron


DOI: 10.1021/jp509557z
J. Phys. Chem. B 2015, 119, 179−191

Table 1. SAXS Fitting Results for CTAC in EAN and Water Systems

| system | concn[a] (wt %) | $SLD_{core}$[b] ($10^{-6}$ Å$^{-2}$) | $SLD_{solvent}$[b] ($10^{-6}$ Å$^{-2}$) | core radius (Å) | length (Å) | $N_{agg}$[c] | micelle fraction[d] (vol %) | shape |
|---|---|---|---|---|---|---|---|---|
| CTAC−EAN | 1 (1.3) | 7.8 | 11.08 | 18.0 ± 0.02 | | 53.3 | | sphere |
| | 3 (3.9) | | | 18.2 ± 0.01 | | 55.1 | 1.6 | sphere |
| | 5 (6.5) | | | 14.6 ± 0.01 | 54.8 ± 0.18 | 80.1 | 9.0 | cylinder |
| | 10 (13) | | | 14.8 ± 0.01 | 56.9 ± 0.11 | 85.5 | 20 | cylinder |
| | 20 (26) | | | 13.5 ± 0.00 | 74.7 ± 0.02 | 93.4 | 32 | cylinder |
| CTAC−water | 1 (1.1) | | 9.45 | 18.9 ± 0.10 | | 61.7 | 0.25 | sphere |
| | 3 (3.3) | | | 19.2 ± 0.01 | | 64.7 | 1.4 | sphere |
| | 5 (5.5) | | | 19.3 ± 0.01 | | 65.7 | 2.3 | sphere |
| | 10 (11) | | | 19.2 ± 0.01 | | 64.7 | 5.2 | sphere |
| | 20 (22) | | | 19.0 ± 0.07 | | 62.7 | 10.0 | sphere |

[a]Values in parentheses are the approximate volume fractions (vol %). [b]Fixed during fitting. [c]Calculated by the volume of the core divided by the individual volume of a $C_{16}$ alkyl chain. Note the $N_{agg}$ value determined here is underestimated. See the Discussion. [d]Micelle fraction derived from the hard sphere interactions.

densities of the relevant parts of the amphiphiles used are calculated as listed in Table S1 in the Supporting Information.

**Structure Factors and Polydispersity.** Structure factors were included to fit the SAXS data for nondilute micellar systems, where the interparticle (micelle) interactions could not be neglected. Either hard sphere or HayterMAS structure interactions were used.[17] Hard sphere structure factors estimate the interparticle structure factor for monodisperse spherical particles interacting through hard sphere (excluded volume) interactions. The calculation uses the Percus−Yevick closure,[40] which was found to be reasonable in most of our systems. HayterMAS structure factors calculate the structure factor (the Fourier transform of the pair correlation function $g(r)$) for charged micelles in a medium.[41,42] When combined with an appropriate form factor (such as a sphere, a core + shell, and an ellipsoid), this allows for inclusion of the interparticle interference effects due to screened Coulomb repulsion between charged particles. This approach only works for charged particles where close contact is unlikely to occur due to the electrostatic repulsions. HayterMAS structure factors were only used for the two cationic surfactants in this work.

Due to the polydispersity (PD) of the copolymer P123, we found it was best to include a polydispersity factor to fit the data. We use Gaussian size distribution to account for the PD of the cores:

$$f(R) = \frac{1}{\sigma\sqrt{2\pi}} \exp\left[-\frac{1}{2\sigma^2}(R - R_{av})^2\right] \quad (3)$$

where $R$ and $R_{av}$ are respectively the radius and the mean radius of the micelles and $\sigma$ is the standard deviation, and then PD can be calculated by $\sigma/R_{av}$.

## RESULTS

The four amphiphiles CTAC, HDPB, Brij 97, and P123 were studied in EAN and water by SAXS at concentrations of 1, 3, 5, 10, and 20 wt %. The scattering patterns were acquired at 45 °C for the CTAC and HDPB systems and 25 °C for the Brij 97 and P123 systems. The higher temperatures were required for CTAC and HDPB since they were insoluble in EAN and in water, respectively, at 25 °C.

**Cationic Amphiphiles in EAN and Water.** *CTAC−EAN and CTAC−Water.* The SAXS patterns for CTAC concentrations of 1, 3, 5, 10, and 20 wt % in EAN and water are shown in Figure 1. The solid lines show the fits to the data. The fitting parameters for CTAC−EAN and CTAC−water are summarized in Table 1.

For CTAC in EAN (Figure 1a), a broad peak is present in the SAXS patterns at 5, 10, and 20 wt %. This peak becomes narrower with increasing concentration and is due to the interparticle (micellar) interactions rather than the structure of the micelles. This scattering feature is consistent with observations in the literature.[20,21] The same trend is observed in water but at lower CTAC concentrations (Figure 1b), which is due to the lower cmcs in water than in EAN. The cmc for CTAC in water at room temperature is 0.042 wt %.[43] It is expected that the cmc for CTAC will be higher in EAN as hexadecyltrimethylammonium bromide (CTAB), the bromide analogue of CTAC, has a cmc value of 0.068 wt % in EAN.[15] Hence, more micellar particles are present in water than in EAN, which leads to higher interparticle interactions.

The SAXS data for 1 wt % CTAC in EAN were best fitted by a spherical model, with no structure factor required. However, when the CTAC concentration was increased to 3 or 5 wt %, a structure factor for hard sphere interactions was required. CTAC formed cylindrical micelles in EAN at concentrations of 5, 10, and 20 wt % (Figure 1a). The enhanced peak with increasing concentrations corresponded to stronger interactions between micelles. The derived volume fractions from the structure factor are slightly larger than the actual volume fractions expected of the starting surfactants as the surfactant micelles are solvated to some extent, particularly the polar headgroups. Therefore, these values are reasonable, which further supports the necessity to use the structure factor.

The SAXS data of CTAC in water were best fitted by a HayterMAS structure factor which relates to the interactions of charged particles. This is due to the intermicellar interactions between the positively charged headgroups of CTAC. The SAXS data for micelles formed by ionic surfactants in the aqueous system were reasonably fitted when considering the interactions between the charged particles.[44−46] In EAN, the ionic nature of the liquid provided shielding of the headgroup charges; therefore, Coulombic interactions between micelles were negligible in EAN, and consequently a hard sphere interaction was most suitable.

It appears that the radius of the micelles remains relatively constant with increasing concentration from 1 to 5 wt %. The radius of the micelles mainly depends on the effective chain length of the hydrophobic (solvophobic) tail, but it should not


DOI: 10.1021/jp509557z
J. Phys. Chem. B 2015, 119, 179−191

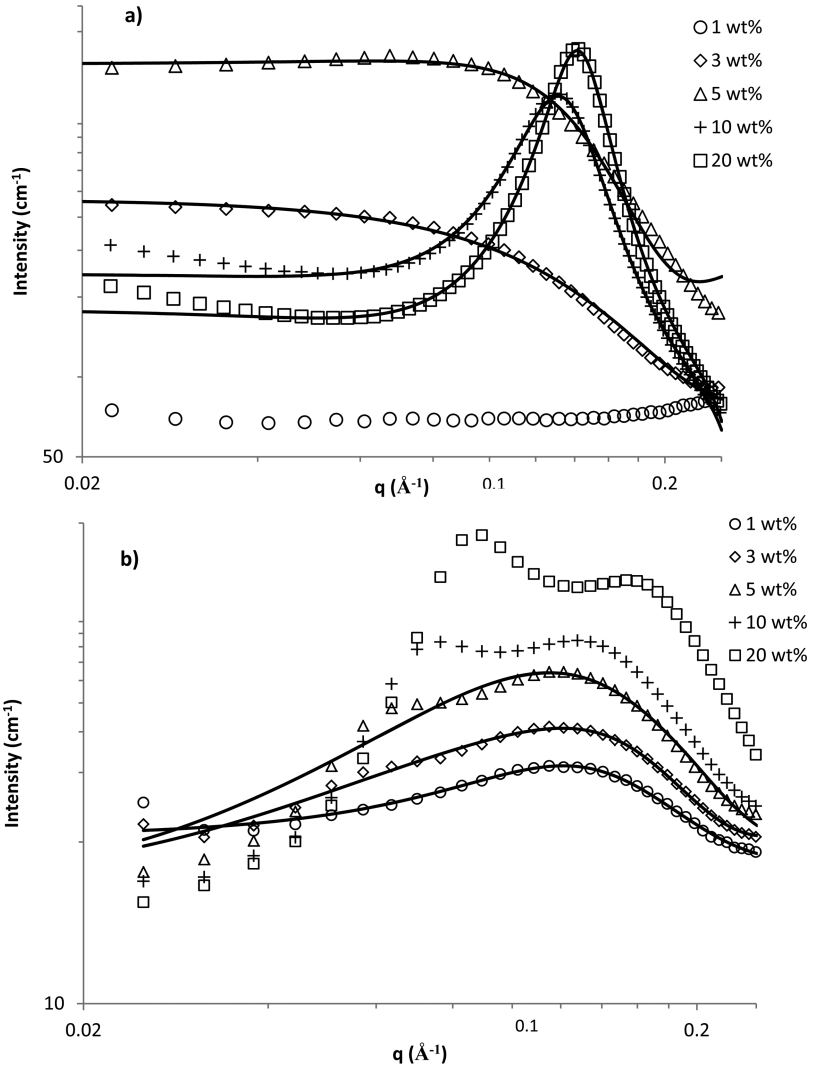


**Figure 2.** SAXS patterns for HDPB concentrations of 1, 3, 5, 10, and 20 wt % in (a) EAN and (b) water at 45 °C. The solid lines show the fits to the data. The 10 and 20 wt % samples in water could not be fitted.

**Table 2. SAXS Fitting Parameters for HDPB in EAN and Water Systems**

| system | concn[a] (wt %) | $SLD_{core}$[b] ($10^{-6}$ Å$^{-2}$) | $SLD_{solvent}$[b] ($10^{-6}$ Å$^{-2}$) | core radius (Å) | length (Å) | $N_{agg}$[c] | micelle fraction[d] (vol %) | shape |
|---|---|---|---|---|---|---|---|---|
| HDPB−EAN | 1 (1.3) | 7.8 | 11.08 | | | | | |
| | 3 (3.9) | | | 17.5 ± 0.01 | | 49.0 | | sphere |
| | 5 (6.5) | | | 14.0 ± 0.03 | 20.7 ± 0.02 | 54.8 | 5.8 | ellipsoid |
| | 10 (13) | | | 11.6 ± 0.01 | 79.7 ± 0.03 | 79.7 | 35 | cylinder |
| | 20 (26) | | | 10.7 ± 0.00 | 82.8 ± 0.04 | 82.8 | 42 | cylinder |
| HDPB−water | 1 (1.1) | | 9.45 | 16.5 ± 0.13 | | 41.1 | 4 | sphere |
| | 3 (3.3) | | | 16.5 ± 0.11 | | 41.1 | 8.9 | sphere |
| | 5 (5.5) | | | 16.9 ± 0.02 | | 44.1 | 15 | sphere |

[a]Values in parentheses are the approximate volume fractions (vol %). [b]Fixed during fitting. [c]Calculated by the volume of the core divided by the individual volume of a $C_{16}$ alkyl chain. Note the $N_{agg}$ value determined here is underestimated; see the Discussion. [d]Micelle fraction derived from the hard sphere interactions.

be greater than its fully extended length, $l_{max}$, which can be estimated using the following equation:[47]

$$l_{max} = 1.5 + 1.265n \quad (4)$$

where $n$ represents the number of carbon atoms in the hydrocarbon chain of the amphiphile that are contained in the hydrocarbon core. For CTAC, $n$ = 16 and the extended chain length is estimated to be 21.7 Å using eq 4. It was revealed by the fitting parameters that the radii (effective chain lengths) of all systems were slightly smaller than their extended chain lengths. This could be due to the first methyl groups next to the hydrophilic (solvophilic) headgroups being solvated by the solvent[44] or the alkyl chain being in a flexible conformation,[23] or most likely it is a combination of both effects. The micelle radii are smaller in EAN than in water, leading to a smaller aggregation number in EAN as presented in Table 1. This


DOI: 10.1021/jp509557z
J. Phys. Chem. B 2015, 119, 179−191

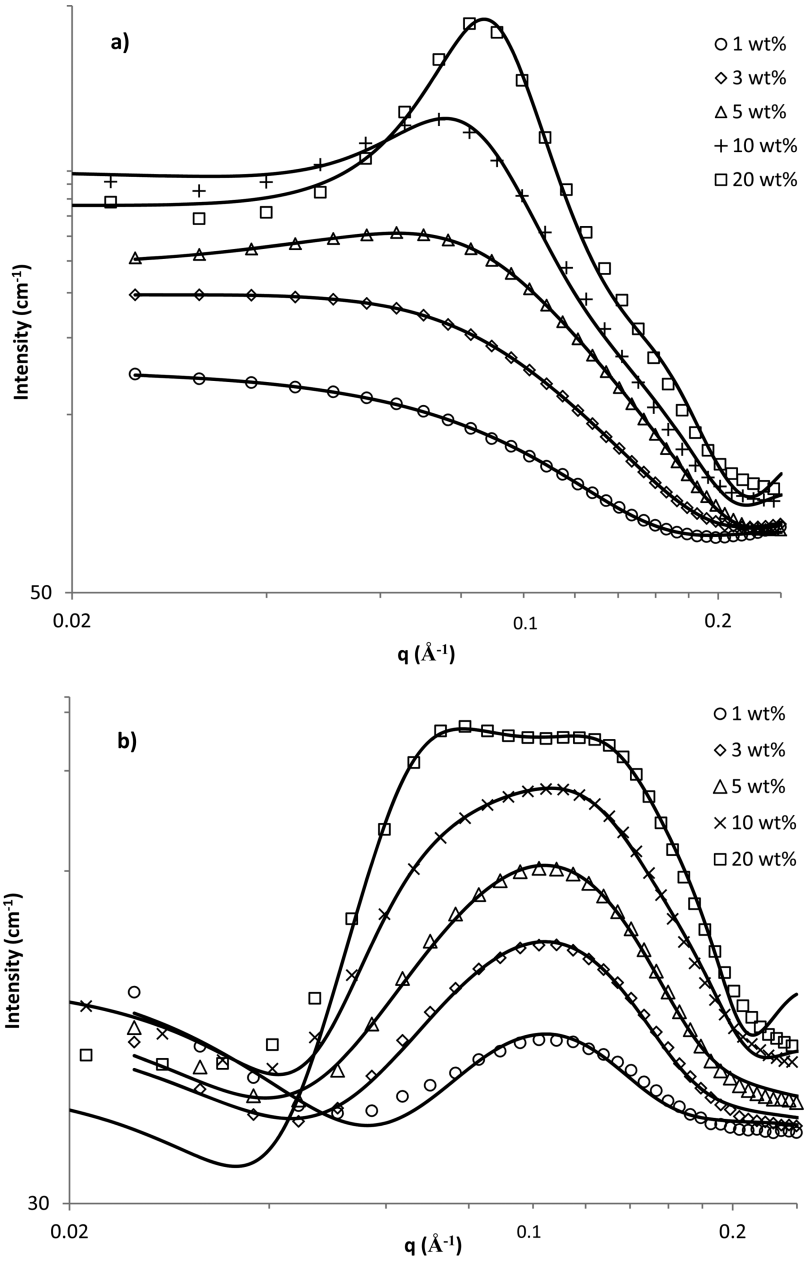


**Figure 3.** SAXS patterns for 1, 3, 5, 10, and 20 wt % Brij 97 in (a) EAN and (b) water at 25 °C. The solid lines show the fits to the data.

could be explained by EAN being a better solvent for the hydrocarbons. Thus, the micelles in EAN are more likely to be infused with EAN molecules, decreasing the SAXS contrast between the micelle and solvent (see the Discussion).

CTAC micelles changed from spherical to cylindrical by 5 wt % CTAC in EAN. There was an increase in the length of cylinders of CTAC in EAN from 5 to 20 wt %, along with a slight decrease in radius. At higher CTAC concentrations (>5 wt %), the counterions are more likely to be associated with the headgroups, thereby reducing the repulsion between the ionic headgroups. This leads to a reduced interfacial area between the headgroups and the solvent (reduced curvature),[48] which promotes the formation of cylinder (rodlike) micelles. This sphere-to-rod transition can occur at lower surfactant concentrations when a salt is present in the aqueous system to reduce the repulsion between the headgroups.[49]

*HDPB—EAN and HDPB—Water.* The SAXS data of HDPB at various concentrations in EAN and water are shown in Figure 2, and their fitting parameters are listed in Table 2.

The SAXS data of HDPB in EAN and water were fitted in the same manner as for the CTAC systems. The very weak scattering for 1 wt % HDPB in EAN could not be fitted, indicating no micelles were present, which is consistent with the cmc value reported for HDPB in EAN at 50 °C of 3.4 wt % (1.69 mM).[15] Since the SAXS patterns were acquired at 45 °C, it is expected that the cmc will be slightly less than 3.4 wt %, since the cmc increases with increasing temperature.[50] For HDPB concentrations of 10 and 20 wt % in EAN, the scattering was very intense and formed a peak at higher $q$ compared to the scattering for 5 wt % HDPB. The sphere model was no longer valid for these two samples. The shift of the peak position also indicated a change of the micellar shape, and a cylinder model fits well for the 10 and 20 wt % samples, as shown in Figure 2a.



DOI: 10.1021/jp509557z
J. Phys. Chem. B 2015, 119, 179−191

Table 3. SAXS Fitting Results for Brij 97 in EAN and Water Systems

| system | concn[a] (wt %) | $SLD_{core}$[b] ($10^{-6}$ Å$^{-2}$) | $SLD_{solvent}$[b] ($10^{-6}$ Å$^{-2}$) | $SLD_{shell}$[c] ($10^{-6}$ Å$^{-2}$) | core radius (Å) | shell thickness (Å) | length (Å) | $N_{agg}$[d] | micelle fraction[e] (vol %) | shape |
|---|---|---|---|---|---|---|---|---|---|---|
| Brij 97−EAN | 1 (1.2) | 7.9 | 11.08 | 10.86 | 23.9 ± 0.1 | 14.5 ± 0.38 | | 111.9 | | sphere |
| | 3 (3.6) | | | 10.90 | 20.5 ± 4.34 | 13.4 ± 0.24 | | 70.6 | | sphere |
| | 5 (6.0) | | | 10.94 | 19.1 ± 0.02 | 14.4 ± 0.03 | | 57.1 | 8 | sphere |
| | 10 (12) | | | 10.89 | 19.8 ± 0.01 | 15.4 ± 0.01 | | 63.6 | 16 | sphere |
| | 20 (24) | | | 10.86 | 20.1 ± 0.01 | 14.6 ± 0.01 | | 66.5 | 29 | sphere |
| Brij 97−water | 1 (1) | | 9.45 | 10.11 | 17.8 ± 0.27 | 21.5 ± 0.45 | | 46.2 | | sphere |
| | 3 (3) | | | 9.82 | 17.9 ± 0.03 | 21.9 ± 0.06 | | 47.0 | | sphere |
| | 5 (5) | | | 9.67 | 19.1 ± 0.02 | 22.6 ± 0.07 | | 57.1 | 8 | sphere |
| | 10 (10) | | | 9.56 | 16.5 ± 0.03 | 18.9 ± 0.07 | 48.3 | 80.8 | 14 | cylinder |
| | 20 (20) | | | 9.89 | 16.3 ± 0.01 | 15.7 ± 0.02 | 70.3 | 116.2 | 20 | cylinder |

[a]Values in parentheses are the approximate volume fractions (vol %). [b]Fixed during fitting. [c]Obtained from fitting. [d]Calculated by the volume of the core divided by the individual volume of a $C_{18}$ alkyl chain. [e]Micelle fraction derived from the hard sphere interactions.

Interestingly, we find that the 5 wt % HDPB in EAN could be best fitted by an ellipsoid model (though it could be fitted with a sphere model), indicating micelle elongation starts at 5 wt %.

The SAXS data for the 1, 3, and 5 wt % HDPB samples in water were fitted with a sphere model using the HayterMAS structure factor (Figure 2b), similar to that of CTAC in water. However, it was not possible to fit the SAXS data of 10 and 20 wt % HDPB in water, most likely due to the strong interactions between the micelles as evident by two scattering peaks (see Figure 2b). The first peak (higher $q$) relates to the structure of the micelles, and the second peak (lower $q$, also known as a correlation peak) mainly relates to the strong interactions between the micelles. This indicated that the SAXS models were valid over the HDPB concentration range used in EAN but not for water at concentrations above 10 wt %. As a result, satisfactory fitting parameters for the 10 and 20 wt % samples were not available using the current model, and the shape and size of the micelles in water could not be obtained. A suitable model that can deal with such strong interparticle interactions is needed for these HDPB samples. However, the correlation peak shifts to high $q$ with increasing concentration, indicating the distance ($L = 2\pi/q$) between the micelles is smaller. The stronger interactions of HDPB in water compared to CTAC in water were due to the lower cmc for HDPB in water (0.81[51] vs 1.94[52] mM at 45 °C). The lower cmc indicates more micelles could form in the HDPB−water system, thus leading to higher intermicellar interactions. The SAXS results of HDPB were consistent with a higher cmc in EAN than in water (less interparticle interactions in EAN at the same concentration).[15,27]

The radius (therefore, the aggregation number) of the HDPB spherical micelles is also independent of the amphiphile concentration. The radius of the HDPB micelles in EAN was slightly larger compared to that reported by light scattering (14.2 Å) in the literature.[27] This difference is probably due to the different characterization techniques. The micelle radius of HDPB also did not exceed the fully extended chain length (21.74 Å) and was smaller compared to that of CTAC micelles. This might be attributed to the difference in headgroups (planar headgroup of HDPB vs globular headgroup of CTAC). The micelle size in water is also noticeably smaller than that in EAN, similar to the CTAC systems, which is due to the higher hydrocarbon solubility in EAN.

Similar to CTAC, the HDPB micelles changed from spherical to cylindrical at high concentrations, from 10 wt % in EAN. There was also a notable reduction in the radius from spherical to cylindrical, implying there was a change in the packing of the amphiphiles. The length of cylinders of HDPB in EAN increased from 79.7 Å at 10 wt % to 82.8 Å at 20 wt % with increasing HDPB concentration, accompanied by a decrease in radius.

**Nonionic Amphiphiles in EAN and Water.** *Brij 97−EAN and Brij 97−Water.* The SAXS patterns for 1, 3, 5, 10, and 20 wt % Brij 97 in EAN and water are shown in Figure 3, and the fitting parameters are summarized in Table 3.

The SAXS patterns for the Brij 97 systems in either solvent could not be fitted by a simple sphere model, and instead the best fits were obtained using core−shell models for spheres or cylinders, depending on the concentration. Brij 97 contains a polar poly(ethylene oxide) ($EO_{10}$) headgroup and a nonpolar hydrocarbon tail group. The EO headgroups are solvophilic, and the hydrocarbon tail groups are solvophobic. Therefore, the micelles were comprised of a hydrocarbon core surrounded by an EO shell.

SAXS patterns for concentrations of Brij 97 above 5 wt % in EAN have a broad peak present due to intermicellar interactions, and a structure factor is required to fit these patterns. All patterns from 1 to 20 wt % were fitted by a core−shell sphere model. For water, the samples at 1, 3, and 5 wt % were best fitted by a core−shell sphere model, and the samples at 10 and 20 wt % were best fitted by a core−shell cylinder model, indicating the transition from spheres to cylinders occurred in water. Velinova et al. also reported the sphere-to-rod transition by a nonionic amphiphile, $C_{12}E_5$, in water at high concentrations.[53] Similarly, the lyotropic liquid crystalline phases formed in water occurred at much lower concentrations than in EAN.[30] The core−shell structure in water was in good agreement with that of Brij 35 reported in the literature.[24] The volume fractions derived from the structure factor for the samples in both EAN and water are in good agreement with the expected values (larger than the actual volume of amphiphiles due to the solvation of the shells), which indicates the excluded volume (hard sphere) interactions are sufficient for these systems.

It was reported that the cmc of the comparable nonionic amphiphile $C_{12}E_5$ was 1.05 wt % in EAN,[12] whereas it was only 0.002 wt % in water.[54] Consequently, the radius is unexpectedly larger at 1 wt % Brij 97 in EAN because it is close to the cmc (weak scattering). This is consistent with the previously reported fitting of SANS patterns for the $C_mE_n$ series in EAN.[11] It was previously reported that the shell thickness of $EO_5$ in EAN was 6.6 Å,[11] and that of $EO_{19}$ in EAN was 32 Å.[55]



DOI: 10.1021/jp509557z
J. Phys. Chem. B 2015, 119, 179−191

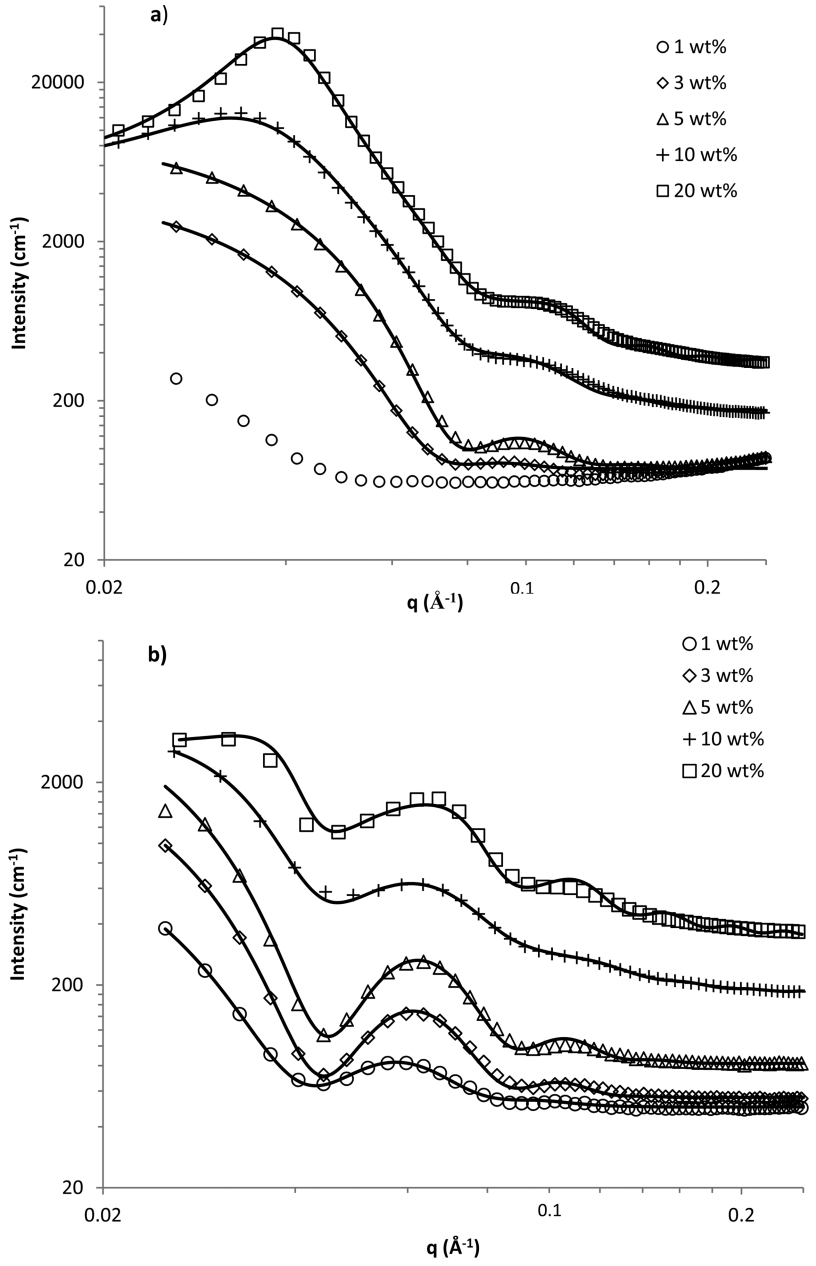


**Figure 4.** SAXS patterns for 1, 3, 5, 10, and 20 wt % P123 in (a) EAN and (b) water at 25 °C. The solid lines show the fits to the data.

**Table 4. SAXS Fitting Results for P123 in EAN and Water Systems**

| system | concn[a] (wt %) | $SLD_{core}$[b] ($10^{-6}$ Å$^{-2}$) | $SLD_{solvent}$[b] ($10^{-6}$ Å$^{-2}$) | $SLD_{shell}$[c] ($10^{-6}$ Å$^{-2}$) | core radius (Å) | shell thickness (Å) | $N_{agg}$[d] | micelle fraction[e] (vol %) | PD |
|---|---|---|---|---|---|---|---|---|---|
| P123−EAN | 1 (1.2) | 9.48 | 11.08 | | | | | | |
| | 3 (3.5) | | | 10.40 | 51.0 ± 0.41 | 21.7 ± 0.52 | 82.6 | | 0.13 |
| | 5 (5.9) | | | 10.88 | 52.4 ± 0.08 | 21.0 ± 0.2 | 89.9 | | 0.06 |
| | 10 (11.7) | | | 10.94 | 53.6 ± 0.03 | 26.5 ± 0.07 | 95.9 | 17 | 0.17 |
| | 20 (23.4) | | | 10.91 | 52.3 ± 0.02 | 25.5 ± 0.03 | 89.1 | 31 | 0.14 |
| P123−water | 1 (1.0) | | 9.45 | 10.90 | 51.6 ± 0.11 | 35.8 ± 1.1 | 85.6 | | 0.18 |
| | 3 (2.9) | | | 11.00 | 51.5 ± 3.03 | 34.4 ± 3.98 | 85.1 | | 0.11 |
| | 5 (4.9) | | | 11.00 | 52.1 ± 0.22 | 31.5 ± 0.3 | 88.1 | | 0.11 |
| | 10 (9.8) | | | 10.30 | 53.4 ± 0.14 | 21.7 ± 0.12 | 94.7 | 17 | 0.20 |
| | 20 (19.6) | | | 10.90 | 60.0 ± 0.03 | 20.7 ± 0.05 | 134.6 | 36 | 0.13 |

[a]Values in parentheses are the approximate volume fractions (vol %). [b]Fixed during fitting. [c]Obtained from fitting. [d]Calculated by the volume of the core divided by the individual volume of a PPO block. [e]Micelle fraction derived from the hard sphere interactions.



DOI: 10.1021/jp509557z
J. Phys. Chem. B 2015, 119, 179−191

This is consistent with the ~15 Å in this work for the average $EO_{10}$ present in Brij 97.

For the aqueous system, the shell was solvated by water as the SLD of the shell is close to that of water, while the hydrocarbon core remained essentially dry.[22] The thickness of the EO shell in water was much larger compared to that in EAN, due to water being a better solvent for the PEO polymer. Therefore, the PEO chains are more compact in EAN.[56] The core radius of the micelles was slightly smaller in water compared to that in EAN (higher hydrocarbon solubility in EAN), but neither exceeded the maximum hydrocarbon tail extended length (24.3 Å). The core radius composed of the $C_{18}$ chain shown in Table 3 was in good agreement with that of analogous surfactants in water[23] and EAN.[11] The core radius is relatively independent of the Brij 97 concentration, which determines the aggregation number. The slightly higher value of the radius for the 5 wt % Brij 97 in water is due to the fact that the shape at this concentration may no longer be spherical. Preu et al. found that the radius of Brij 35 in water increased from 16.9 Å at 3.6 wt % Brij 35 to 19.6 Å at 6.0 wt % Brij 35.[22]

*P123–EAN and P123–Water.* The SAXS patterns for 1, 3, 5, 10, and 20 wt % P123 in EAN and in water are shown in Figure 4, and the fitting parameters are summarized in Table 4.

All the SAXS patterns for the P123 samples in EAN and in water were fitted using a spherical core–shell model, except the 1 wt % P123 in EAN. The negligible scattering for this system indicated no micelles were present (or too few) at that concentration. The 3 and 5 wt % samples were fitted without a structure factor, due to the minimal intermicellar interactions. However, a structure factor was required for P123 concentrations of 10 and 20 wt % due to the strong intermicellar interactions. Similar trends are observed for the water–P123 samples. The fitted volume fractions in both EAN and water seemingly are much larger than their starting volumes, which is due to the fact the EO shells are highly solvated. Manet et al. reported that the shell in the P123–water system can contain up to 90% solvent.[57]

The P123 polymer consists of two symmetric PEO groups and one PPO group. The fitting parameters of the core–shell structure of micelles formed in water in this work are consistent with literature values.[58] Lam et al.[59] reported the direct visualization of the micelles of Pluronic block polymers in water by cryo-TEM and confirmed their spherical shape. It should be noted that there is a broad peak around $q$ = 0.06 $Å^{-1}$ and a shoulder peak around $q$ = 0.12 $Å^{-1}$ in water that is enhanced with increasing P123 concentration. These peaks are mainly attributed to the intermicellar interactions. Such enhanced peaks, in particular the shoulder peaks, are not obvious in EAN. The cmcs for the nonionic block copolymer exhibit an order of magnitude difference between EAN and water. This implies that there are differences in the micellar interactions between the two solvents, at least for the concentrations under study.

The core radii of micelles formed by P123 in EAN and water are quite large, ~52 Å, due to the size of the PPO group, but are independent of the P123 concentration or solvent. This means that the PPO block has similar solubilities in EAN and water, which was consistent with the literature findings.[24] However, there is a slight increase in radius in water at higher concentrations (>10 wt %). The larger radius obtained at 20 wt % P123 in water, and therefore larger aggregation number, is most likely due to the growth of micelles at such high concentration.

Similar to that of the Brij 97 system, the shell thickness in EAN was much smaller than that in water, which indicates that water is a better solvent for PEO; hence, the PEO chains are more extended in water. The PD of the core size is within expected values, ranging from 0.1 to 0.2.

## DISCUSSION

**Effects of Electron Densities for the SAXS Fitting.** The scattering in SAXS patterns for micellar systems occurs due to the electron density differences between the core and the shell and between the shell and the solvent. Consequently, larger differences in the electron densities between the amphiphiles and the solvents lead to better contrast and more intense scattering. There was no apparent scattering due to the shell region for micelles of the cationic surfactants, indicating no contrast between the shell and the solvent. Scattering models for spherical, ellipsoidal, and cylindrical micelles, with and without core–shell structure, were trialed, and meaningful fits were only obtained without the core–shell structure. To some extent, this is due to the similarity in chemical structure of the headgroups of the cationic surfactants and EAN and their similar electron density values. The electron densities for the CTAC headgroup (324 e/$nm^3$) and the HDPB headgroup (313 e/$nm^3$) are distinctive from those for the hydrocarbon chains and the solvents (393 e/$nm^3$ for EAN and 334 e/$nm^3$ for water). However, it is anticipated that a larger scattering effect in EAN is due to some of the EAN behaving as a cosurfactant, with the ethyl chain orientated within the micelle core and the ammonium group located within the ionic shell. Additional EAN ions will solvate the cationic headgroups, providing electrostatic shielding, and will also be present within the micelle headgroup region, further decreasing the contrast compared to the bulk EAN. Competitive counterion exchange is another factor to consider.[37] The nitrate counterion in the EAN will exchange with the counterion of both the CTAC and HDPB micelles. This will also potentially contribute to a lower contrast between the Stern layer and the surrounding ionic liquid. It is believed that the core remains relatively "dry", though the methyl group next to the headgroup may also be solvated to some extent. Consequently, the electron density contrast was predominantly between the core and the ionic headgroup region for the two cationic surfactants and was best fitted by a simple sphere model.

The nonionic amphiphiles had a smaller difference between the electron densities of the headgroup region (394 e/$nm^3$) and EAN (393 e/$nm^3$). However, it seems there was sufficient contrast with the aid of a powerful synchrotron light such that the SAXS patterns were best fitted using core–shell models. The single sphere model (with a shell) did not fit the data well, and the comparison of the fitting with and without a shell is shown in the Supporting Information (Figure S1). The nonionic amphiphiles of P123 and Brij 97 had substantially larger headgroups than the cationic surfactants, and hence, much thicker shell layers were expected, which will assist the scattering contrast. We anticipate that the EO shells are highly solvated with the chains being in a random flight chain conformation in the solvent. However, as water is a better solvent for EO blocks, the chains are more extended than those in EAN as one can expect. The fitting parameters for the micelle cores are expected to be representative of the actual micelle core sizes and shapes due to the strong electron density contrast between the hydrocarbon core and the polar headgroup region.


DOI: 10.1021/jp509557z
J. Phys. Chem. B 2015, 119, 179–191

**Aggregation Number of Cationic Surfactants.** The aggregation numbers ($N_{agg}$) for the cationic surfactants CTAC and HDPB are smaller than those reported in the literature, which to a large extent we attribute to the artifact of the SAXS technique where the electron density contrast results in an underestimation of the radius. The $N_{agg}$ for CTAC in water at 25 °C was reported to be 80.7 by a static light scattering technique,[60] and the $N_{agg}$ for cetylpyridinium chloride (CPC), analogous to HDPB (same headgroup and alkyl chain length), in water at 25 °C was determined to be 52 by a stepwise thinning process of foam films.[61] Our $N_{agg}$ values for these surfactants are ∼65 for CTAC and ∼41 for HDPB, indicating the core radius we fitted is smaller than the literature values. Hayter and Penfold, using small-angle neutron scattering, showed that the charged cationic micelles in water were composed of a hydrocarbon core and a shell consisting of the solvated headgroups and a portion of the methyl groups next to the headgroups.[44] In our approach (using SAXS data), we are only able to examine the dry hydrocarbon core, which underestimates the actual radius of the micelle size, therefore obtaining smaller aggregation numbers. Table 5 lists the adjusted $N_{agg}$ (calculated by adjusting the number of carbons in the core) for the spherical micelles for the CTAC and HDPB systems. The adjusted $N_{agg}$ is comparable to the literature values when $n$ is 14 as shown in Table 5 (two methyl groups in the polar solvation shell) given the fact that the $N_{agg}$ should be lower at 45 °C compared to that at 25 °C.[62] This is reasonable as the solvent (water or EAN) can penetrate into the micelle due to the fact that there is repulsion between the charged groups.

**Table 5. Adjusted Aggregation Numbers for the Spherical Micelles for the CTAC and HDPB Systems**

| system | concn (wt %) | $N_{agg}$ ($n$ = 16)[a] | $N_{agg}$ ($n$ = 15)[a] | $N_{agg}$ ($n$ = 14)[a] |
|---|---|---|---|---|
| CTAC−EAN | 1 | 53.3 | 56.7 | 60.4 |
| | 3 | 55.1 | 58.6 | 62.5 |
| CTAC−water | 1 | 61.7 | 65.6 | 70.0 |
| | 3 | 64.7 | 68.8 | 73.3 |
| | 5 | 65.7 | 69.8 | 74.5 |
| | 10 | 64.7 | 68.8 | 73.3 |
| | 20 | 62.7 | 66.6 | 71.1 |
| HDPB−EAN | 3 | 49.0 | 52.1 | 55.4 |
| HDPB−water | 1 | 41.1 | 43.6 | 46.6 |
| | 3 | 41.1 | 43.6 | 46.6 |
| | 5 | 44.1 | 46.9 | 50.0 |

[a] $n$ is the number of hydrocarbons in the alkyl chain contributing to the core.

To re-evaluate if the shape of the cationic surfactant micelles is spherical and the size of the hydrocarbon core, we refit the SAXS data with a simple body-centered cubic (bcc) lattice model. In this model, the spheres are packed in a bcc lattice. Strikingly, all CTAC data in water (from 1 to 20 wt %), 1 and 3 wt % CTAC in EAN, 1 and 3 wt % HDPB in water, and 3 wt % HDPB in EAN fitted this model quite well (see the Supporting Information, Figure S2). The radius (listed in the Supporting Information, Table S3) of the spheres agrees well with the values in the tables (Tables 1 and 2), and the distance between the spheres decreases with increasing surfactant concentration. The size of the micelles in EAN appears to be smaller, which is expected due to the weaker solvophobic forces in EAN.[27] All other shapes (cylinder and ellipsoid) could not be fitted with the bcc model. This is consistent with the consideration that the solvation shell could not be differentiated from the solvent background by SAXS due to the weak contrast in the scattering length densities between the hydrocarbon core ($7.8 \times 10^{-6}$ Å$^{-2}$) and water ($9.45 \times 10^{-6}$ Å$^{-2}$). Alternative techniques such as SANS may give details of the shell due to an enhanced contrast (e.g., in a deuterated solvent).

**Solvophobic Effect Differences between Water and EAN.** A key solvent characteristic that promotes a good amphiphile self-assembly medium is a high cohesive energy density. This is enhanced by hydrogen bonding, and both water and EAN are capable of forming three-dimensional hydrogen-bonded networks.[63] However, compared to water, EAN has an ethyl moiety on the cation, which leads to the formation of liquid intermediate range order polar and nonpolar segregated domains for neat EAN.[64] The presence of the nonpolar region increases the solubility of hydrocarbons through increased van der Waals interactions and hence impacts the solvophobic effect, and results in higher cmc values in EAN compared to water.[65] From the combination of the intermicellar information along with the limited cmc data available for the systems investigated, it was evident that the cationic amphiphiles of CTAC and HDPB had cmcs in EAN that were closer to those in water, typically a factor of 2−3 larger. In contrast, nonionic amphiphiles analogous to Brij 97 have cmcs which are typically 5 orders of magnitude larger in EAN than in water.[12] These large differences in cmcs for ionic and nonionic amphiphiles is predominantly due to two competing factors. First, there is a lower hydrocarbon solubility in EAN than in water, which decreases the solvophobic effect for all amphiphiles in EAN. Second, there is an effective shield of the electrostatic repulsion between the cationic surfactant headgroups in EAN which favors micellization for ionic surfactants. The overall effect of these competing factors is that the solvophobic effect is greater in water than in EAN, and due to electrostatic shielding the solvophobic effect is greater for ionic surfactants compared to nonionic amphiphiles in EAN.

The charged amphiphiles in water have a HayterMAS structure factor, whereas the nonionic surfactants in water and all surfactants in EAN have a hard sphere factor.[66] Only the ionic surfactants in water will behave as charged blobs and consist of two opposing forces, from the headgroup charge repulsion and the van der Waals attractions.[67] In EAN the charge screening is so effective due to the ionic nature of the solvent that the micelles are best treated as uncharged. The lower cmc values in water led to more micelles at these concentrations compared to those in EAN. Most of the water−amphiphile SAXS patterns fitted well when the HayterMAS structure factor was included. The exceptions were the 10 and 20 wt % HDPB samples in water, which could not be fitted by using the HayterMAS or the hard sphere factor. The lower cmc of HDPB in water leads to formation of spheres, impacting the validity of the scattering models.

**Micelle Shape, Packing Parameters, and Headgroup Areas.** Spherical micelles were favored by all the amphiphiles in EAN or water at the lower concentrations used. This is consistent with the geometrical shape of the amphiphiles where global packing constraints have a negligible influence.[28] The spherical micelles became cylindrical with increasing concentration for the CTAC, HDPB, and Brij 97 amphiphiles in water and EAN. Previously we have reported the lyotropic liquid crystal phases present for CTAC, HDPB, and Brij 97 in water


DOI: 10.1021/jp509557z
J. Phys. Chem. B 2015, 119, 179−191

and EAN, with hexagonal and lamellar phases present.[30] In contrast, the micelles of P123 retained their spherical structure in EAN or water from 1 to 20 wt % P123. Therefore, P123 in EAN or in water has a strong preference for the high curvature of the spherical phase, and the transition to lower curvature phases must occur at amphiphile concentrations above 20 wt %.

With increasing amphiphile concentration, global constraints can lead to micelles packing into cubic or hexagonal arrangements.[4,34] Further increases in amphiphile concentration may lead to other lyotropic liquid crystal phases in accordance with the standard phase progression.[34] For dilute micelles, where global packing constraints are negligible, the preferred micellar shape is governed by the geometry of the amphiphile in the solvent, using the CPP, as described by eq 1. There was a minimal difference between the effective chain lengths of the hydrocarbon portion of the amphiphiles for the different solvents, as shown from the fits to the SAXS patterns. Therefore, the solvation of headgroups, and hence the headgroup area, is dominant in determining the micellar characteristics and which liquid crystalline phases are present for higher amphiphile concentrations. The effective headgroup area, *a*, refers to the area occupied by the molecule at the solvent and surfactant interface, with a larger headgroup area (higher curvature) usually leading to more diverse phases.

The estimated headgroup areas for CTAC, HDPB, and Brij 97 in EAN and water are provided in the Supporting Information (Table S2). The nature of the solvent leads to a difference in the amphiphile headgroup areas in EAN and water. EAN as a structured solvent[68] has higher alkyl solubility than water and as a consequence less solvophobicity for the amphiphile molecules. Thus, larger headgroup areas (higher curvature) are expected in water due to more solvation. However, the headgroup areas were larger in water for CTAC and Brij 97 but smaller for HDPB and P123. This is indicative of the complexity of interactions possible between the headgroups and the EAN ions. It appears that EAN solvates the HDPB to a relatively greater extent than CTAC, at least in comparison to water. The phase sequence of our previous work[30] (see Table S2) is consistent with higher *a* leading to more diverse phases. The headgroup area for the P123 amphiphile in EAN and water was much larger compared to those of other amphiphiles; thus, a discrete cubic phase ($I_1$) was observed before the $H_1$ phase. Similar headgroup areas (curvature) for P123 in EAN and water have resulted in similar phases.[69]

## CONCLUSIONS

The SAXS data of four different types of amphiphiles (CTAC, HDPB, Brij 97, and P123) up to 20 wt % in EAN and water were fitted using various models. In particular, the two cationic surfactants required very different methods to fit their data in EAN compared to water as the charged micelles are shielded in EAN, effectively removing headgroup repulsion. All samples were fitted with a monodisperse micelle model using either spherical or cylindrical form factors, except for the copolymer P123. The quality of the fits obtained indicated that the micelles were relatively monodisperse for these amphiphiles in either EAN or water at the various concentrations. A structure factor was needed to fit the data at higher concentrations due to the intermicellar interactions, which in most cases can be described by the excluded volume interactions. The micelles at low concentrations were generally spheres, which were thermodynamically favorable. The spheres were elongated and transferred into cylinders with increasing amphiphile concentration for those amphiphiles with relatively small headgroup areas (CTAC, HDPB, and Brij 97) at the amphiphile−solvent interface. When such a headgroup area was particularly large (P123), more diverse phases were likely to form. However, in such situations the micellar shape did not transition from spheres to cylinders. A core−shell structure was fitted for the nonionic amphiphiles containing EO groups in both EAN and water. However, due to the poor contrast between the EO shell and the EAN solvent, the thickness of the shell was most likely underestimated.

## ASSOCIATED CONTENT

### Supporting Information

Micelle scattering models, volumes and electron densities of various parts of the amphiphiles and solvents, headgroup area per amphiphile chain of CTAC, HDPB, and Brij 97 at 3 wt % in EAN and water, SAXS curves of CTAC in water, CTAC in EAN, HDPB in water, and HDPB in EAN fitted with a bcc model, and fitting parameters of the systems with a bcc model showing the radius ($R_c$) and distance between the centers of the micelles ($d$). This material is available free of charge via the Internet at http://pubs.acs.org.

## AUTHOR INFORMATION

### Corresponding Authors

*E-mail: rcaruso@unimelb.edu.au.
*E-mail: calum.drummond@rmit.edu.au.

### Notes

The authors declare no competing financial interest.

## ACKNOWLEDGMENTS

C.J.D. and R.A.C. acknowledge receipt of an Australian Research Council (ARC) Federation Fellowship and Future Fellowship (Grant FT0990583), respectively. Z.C. acknowledges a Ph.D. studentship provided by the Commonwealth Scientific and Industrial Research Organization (CSIRO). This work was partly supported by an ARC Discovery Project grant, DP0666961. This research was undertaken in part on the SAXS/WAXS beamline at the Australian Synchrotron (M2147), Victoria, Australia. This work benefitted from software developed by the DANSE project under National Science Foundation (NSF) Award DMR-0520547.

## REFERENCES

(1) Wijaya, E. C.; Greaves, T. L.; Drummond, C. J. Linking molecular/ion structure, solvent mesostructure, the solvophobic effect and the ability of amphiphiles to self-assemble in non-aqueous liquids. *Faraday Discuss.* **2013**, *167*, 191−215.

(2) Khan, A. Phase science of surfactants. *Curr. Opin. Colloid Interface Sci.* **1996**, *1* (5), 614−623.

(3) Greaves, T. L.; Drummond, C. J. Solvent nanostructure, the solvophobic effect and amphiphile self-assembly in ionic liquids. *Chem. Soc. Rev.* **2013**, *42* (3), 1096−1120.

(4) Greaves, T. L.; Drummond, C. J. Ionic liquids as amphiphile self-assembly media. *Chem. Soc. Rev.* **2008**, *37* (8), 1709−1726.

(5) Greaves, T. L.; Weerawardena, A.; Fong, C.; Drummond, C. J. Formation of amphiphile self-assembly phases in protic ionic liquids. *J. Phys. Chem. B* **2007**, *111* (16), 4082−4088.

(6) Evans, D. F. Self-organization of amphiphiles. *Langmuir* **1988**, *4* (1), 3−12.

(7) Hao, J. C.; Hoffmann, H. Self-assembled structures in excess and salt-free catanionic surfactant solutions. *Curr. Opin. Colloid Interface Sci.* **2004**, *9* (3−4), 279−293.



DOI: 10.1021/jp509557z
*J. Phys. Chem. B* 2015, 119, 179−191

(8) Zech, O.; Kunz, W. Conditions for and characteristics of nonaqueous micellar solutions and microemulsions with ionic liquids. *Soft Matter* **2011**, *7* (12), 5507−5513.
(9) Rao, V. G.; Mandal, S.; Ghosh, S.; Banerjee, C.; Sarkar, N. Ionic Liquid-in-Oil Microemulsions Composed of Double Chain Surface Active Ionic Liquid as a Surfactant: Temperature Dependent Solvent and Rotational Relaxation Dynamics of Coumarin-153 in [Py]-[$TF_2N$]/[$C_4$mim][AOT]/Benzene Microemulsions. *J. Phys. Chem. B* **2012**, *116* (28), 8210−8221.
(10) Xie, L.-L. Thermodynamics of AOT Micelle Formation in Ethylammonium Nitrate. *J. Dispersion Sci. Technol.* **2009**, *30* (1), 100−103.
(11) Araos, M. U.; Warr, G. G. Structure of nonionic surfactant micelles in the ionic liquid ethylammonium nitrate. *Langmuir* **2008**, *24* (17), 9354−9360.
(12) Greaves, T. L.; Mudie, S. T.; Drummond, C. J. Effect of protic ionic liquids (PILs) on the formation of non-ionic dodecyl poly(ethylene oxide) surfactant self-assembly structures and the effect of these surfactants on the nanostructure of PILs. *Phys. Chem. Chem. Phys.* **2011**, *13* (45), 20441−20452.
(13) Wakeham, D.; Warr, G. G.; Atkin, R. Surfactant Adsorption at the Surface of Mixed Ionic Liquids and Ionic Liquid Water Mixtures. *Langmuir* **2012**, *28* (37), 13224−13231.
(14) Yue, X.; Chen, X.; Li, Q. Comparison of Aggregation Behaviors of a Phytosterol Ethoxylate Surfactant in Protic and Aprotic Ionic Liquids. *J. Phys. Chem. B* **2012**, *116* (31), 9439−9444.
(15) Evans, D. F.; Yamauchi, A.; Roman, R.; Casassa, E. Z. Micelle Formation in Ethylammonium Nitrate, a Low-Melting Fused Salt. *J. Colloid Interface Sci.* **1982**, *88* (1), 89−96.
(16) Lin, Z.; Cai, J. J.; Scriven, L. E.; Davis, H. T. Spherical-to-wormlike micelle transition in CTAB solutions. *J. Phys. Chem.* **1994**, *98* (23), 5984−5993.
(17) Pedersen, J. S. Analysis of small-angle scattering data from colloids and polymer solutions: modeling and least-squares fitting. *Adv. Colloid Interface Sci.* **1997**, *70*, 171−210.
(18) Pedersen, J. S.; Gerstenberg, M. C. The structure of P85 Pluronic block copolymer micelles determined by small-angle neutron scattering. *Colloids Surf., A* **2003**, *213* (2−3), 175−187.
(19) Galantini, L.; Giglio, E.; Leonelli, A.; Pavel, N. V. An integrated study of small-angle X-ray scattering and dynamic light scattering on cylindrical micelles of sodium glycodeoxycholate. *J. Phys. Chem. B* **2004**, *108* (9), 3078−3085.
(20) Liu, Y. C.; Chen, S. H.; Huang, J. S. Small-angle neutron scattering analysis of the structure and interaction of triblock copolymer micelles in aqueous solution. *Macromolecules* **1998**, *31* (7), 2236−2244.
(21) Perche, T.; Auvray, X.; Petipas, C.; Anthore, R.; Rico, I.; Lattes, A.; Bellissent, M. C. Small-angle neutron and X-ray scattering study of the formation and structure of micelles of CTAB in formamide. *J. Phys. I* **1992**, *2* (6), 923−942.
(22) Preu, H.; Zradba, A.; Rast, S.; Kunz, W.; Hardy, E. H.; Zeidler, M. D. Small angle neutron scattering of $D_2O$-Brij 35 and $D_2O$-alcohol-Brij 35 solutions and their modelling using the Percus-Yevick integral equation. *Phys. Chem. Chem. Phys.* **1999**, *1* (14), 3321−3329.
(23) Sommer, C.; Pedersen, J. S.; Garamus, V. M. Structure and interactions of block copolymer micelles of Brij 700 studied by combining small-angle X-ray and neutron scattering. *Langmuir* **2005**, *21* (6), 2137−2149.
(24) Tomsic, M.; Bester-Rogac, M.; Jamnik, A.; Kunz, W.; Touraud, D.; Bergmann, A.; Glatter, O. Nonionic surfactant Brij 35 in water and in various simple alcohols: Structural investigations by small-angle X-ray scattering and dynamic light scattering. *J. Phys. Chem. B* **2004**, *108* (22), 7021−7032.
(25) Anderson, J. L.; Pino, V.; Hagberg, E. C.; Sheares, V. V.; Armstrong, D. W. Surfactant solvation effects and micelle formation in ionic liquids. *Chem. Commun.* **2003**, No. 19, 2444−2445.
(26) Patrascu, C.; Gauffre, F.; Nallet, F.; Bordes, R.; Oberdisse, J.; de Lauth-Viguerie, N.; Mingotaud, C. Micelles in ionic liquids: Aggregation behavior of alkyl poly(ethyleneglycol)-ethers in 1-butyl-3-methyl-imidazolium type ionic liquids. *ChemPhysChem* **2006**, *7* (1), 99−101.
(27) Evans, D. F.; Yamauchi, A.; Wei, G. J.; Bloomfield, V. A. Micelle Size in Ethylammonium Nitrate as Determined by Classical and Quasi-Elastic Light-Scattering. *J. Phys. Chem.* **1983**, *87* (18), 3537−3541.
(28) Israelachvili, J. N.; Mitchell, D. J.; Ninham, B. W. Theory of self-assembly of hydrocarbon amphiphiles into micelles and bilayers. *J. Chem. Soc., Faraday Trans. 2* **1976**, *72*, 1525−1568.
(29) Ray, A. Solvophobic Interactions and Micelle Formation in Structure Forming Nonaqueous Solvents. *Nature* **1971**, *231* (5301), 313−315.
(30) Chen, Z.; Greaves, T. L.; Fong, C.; Caruso, R. A.; Drummond, C. J. Lyotropic Liquid Crystalline Phase Behaviour in Amphiphile-Protic Ionic Liquid Systems. *Phys. Chem. Chem. Phys.* **2012**, *14* (11), 3825−3836.
(31) Berr, S. S.; Caponetti, E.; Johnson, J. S.; Jones, R. R. M.; Magid, L. J. Small-angle neutro-scattering from hexadecyltrimethylammonium bromide micelles in aqueous solutions. *J. Phys. Chem.* **1986**, *90* (22), 5766−5770.
(32) Asencio, R. A.; Cranston, E. D.; Atkin, R.; Rutland, M. W. Ionic Liquid Nanotribology: Stiction Suppression and Surface Induced Shear Thinning. *Langmuir* **2012**, *28* (26), 9967−9976.
(33) Imae, T.; Ikeda, S. Sphere rod transition of micelles of tetradecyltrimethylammonium halides in aqueous sodium-halide solutions and flexibility and entanglement of long rodlike micelles. *J. Phys. Chem.* **1986**, *90* (21), 5216−5223.
(34) Kaasgaard, T.; Drummond, C. J. Ordered 2-D and 3-D nanostructured amphiphile self-assembly materials stable in excess solvent. *Phys. Chem. Chem. Phys.* **2006**, *8* (43), 4957−4975.
(35) Ma, F. M.; Chen, X.; Zhao, Y. R.; Wang, X. D.; Li, Q. H.; Lv, C.; Yue, X. A Nonaqueous Lyotropic Liquid Crystal Fabricated by a Polyoxyethylene Amphiphile in Protic Ionic Liquid. *Langmuir* **2010**, *26* (11), 7802−7807.
(36) Zhao, Y. R.; Chen, X.; Wang, X. D. Liquid Crystalline Phases Self-Organized from a Surfactant-like Ionic Liquid $C_{16}$mimCl in Ethylammonium Nitrate. *J. Phys. Chem. B* **2009**, *113* (7), 2024−2030.
(37) Greaves, T. L.; Weerawardena, A.; Fong, C.; Drummond, C. J. Many protic ionic liquids mediate hydrocarbon-solvent interactions and promote amphiphile self-assembly. *Langmuir* **2007**, *23* (2), 402−404.
(38) Atkin, R.; Bobillier, S. M. C.; Warr, G. G. Propylammonium Nitrate as a Solvent for Amphiphile Self-Assembly into Micelles, Lyotropic Liquid Crystals, and Microemulsions. *J. Phys. Chem. B* **2010**, *114* (3), 1350−1360.
(39) Greaves, T. L.; Weerawardena, A.; Fong, C.; Krodkiewska, I.; Drummond, C. J. Protic ionic liquids: Solvents with tunable phase behavior and physicochemical properties. *J. Phys. Chem. B* **2006**, *110* (45), 22479−22487.
(40) Percus, J. K.; Yevick, G. J. Analysis of classical statistical mechanics by means of collective coordinates. *Phys. Rev.* **1958**, *110* (1), 1−13.
(41) Hansen, J. P.; Hayter, J. B. A rescaled MAS structure factor for dilute charged colloidal dispersions. *Mol. Phys.* **1982**, *46* (3), 651−656.
(42) Hayter, J. B.; Penfold, J. An analytic structure factor for macroion solutions. *Mol. Phys.* **1981**, *42* (1), 109−118.
(43) Mata, J.; Varade, D.; Bahadur, P. Aggregation behavior of quaternary salt based cationic surfactants. *Thermochim. Acta* **2005**, *428* (1−2), 147−155.
(44) Hayter, J. B.; Penfold, J. Determination of micelle structure and charge by neutron small-angle scattering. *Colloid Polym. Sci.* **1983**, *261* (12), 1022−1030.
(45) Kumar, S.; Sharma, D.; Kabir ud, D. Small-angle neutron scattering studies on sodium dodecylbenzenesulfonate-tetra-n-butylammonium bromide systems. *J. Surfactants Deterg.* **2006**, *9* (1), 77−82.
(46) Haldar, J.; Aswal, V. K.; Goyal, P. S.; Bhattacharya, S. Aggregation properties of novel cationic surfactants with multiple pyridinium headgroups. Small-angle neutron scattering and conductivity studies. *J. Phys. Chem. B* **2004**, *108* (31), 11406−11411.


DOI: 10.1021/jp509557z
*J. Phys. Chem. B* 2015, 119, 179−191

(47) Tanford, C. Micelle shape and size. *J. Phys. Chem.* **1972**, *76* (21), 3020−3024.
(48) Missel, P. J.; Mazer, N. A.; Benedek, G. B.; Young, C. Y.; Carey, M. C. Thermodynamic analysis of the growth of sodium dodecyl sulfate micelles. *J. Phys. Chem.* **1980**, *84* (9), 1044−1057.
(49) Goyal, P. S.; Dasannacharya, B. A.; Kelkar, V. K.; Manohar, C.; Rao, K. S.; Valaulikar, B. S. Shapes and sizes of micelles in CTAB solutions. *Physica B* **1991**, *174* (1−4), 196−199.
(50) Kang, K.-H.; Kim, H.-U.; Lim, K.-H. Effect of temperature on critical micelle concentration and thermodynamic potentials of micellization of anionic ammonium dodecyl sulfate and cationic octadecyl trimethyl ammonium chloride. *Colloids Surf., A* **2001**, *189* (1−3), 113−121.
(51) Yan, J.; Wang, D.; Bu, F.; Yang, F. F. Investigation of the Thermodynamic Properties of the Cationic Surfactant CTAC in EG +Water Binary Mixtures. *J. Solution Chem.* **2010**, *39* (10), 1501−1508.
(52) Jalali, F.; Shamsipur, M.; Alizadeh, N. Conductance study of the thermodynamics of micellization of 1-hexadecylpyridinium bromide in (water plus cosolvent). *J. Chem. Thermodyn.* **2000**, *32* (6), 755−765.
(53) Velinova, M.; Sengupta, D.; Tadjer, A. V.; Marrink, S.-J. Sphere-to-Rod Transitions of Nonionic Surfactant Micelles in Aqueous Solution Modeled by Molecular Dynamics Simulations. *Langmuir* **2011**, *27* (23), 14071−14077.
(54) Lugo, D.; Oberdisse, J.; Karg, M.; Schweins, R.; Findenegg, G. H. Surface aggregate structure of nonionic surfactants on silica nanoparticles. *Soft Matter* **2009**, *5* (15), 2928−2936.
(55) Atkin, R.; De Fina, L. M.; Kiederling, U.; Warr, G. G. Structure and Self Assembly of Pluronic Amphiphiles in Ethylammonium Nitrate and at the Silica Surface. *J. Phys. Chem. B* **2009**, *113* (36), 12201−12213.
(56) Werzer, O.; Warr, G. G.; Atkin, R. Compact Poly(ethylene oxide) Structures Adsorbed at the Ethylammonium Nitrate−Silica Interface. *Langmuir* **2011**, *27* (7), 3541−3549.
(57) Manet, S.; Lecchi, A.; Imperor-Clerc, M.; Zholobenko, V.; Durand, D.; Oliveira, C. L. P.; Pedersen, J. S.; Grillo, I.; Meneau, F.; Rochas, C. Structure of Micelles of a Nonionic Block Copolymer Determined by SANS and SAXS. *J. Phys. Chem. B* **2011**, *115* (39), 11318−11329.
(58) Soni, S. S.; Brotons, G.; Bellour, M.; Narayanan, T.; Gibaud, A. Quantitative SAXS analysis of the P123/water/ethanol ternary phase diagram. *J. Phys. Chem. B* **2006**, *110* (31), 15157−15165.
(59) Lam, Y. M.; Grigorieff, N.; Goldbeck-Wood, G. Direct visualisation of micelles of Pluronic block copolymers in aqueous solution by cryo-TEM. *Phys. Chem. Chem. Phys.* **1999**, *1* (14), 3331−3334.
(60) Imae, T.; Ikeda, S. Characteristics of rodlike micelles of cetyltrimethylammonium chloride in aqueous NaCl solutions: Their flexibility and the scaling laws in dilute and semidilute regimes. *Colloid Polym. Sci.* **1987**, *265* (12), 1090−1098.
(61) Anachkov, S. E.; Danov, K. D.; Basheva, E. S.; Kralchevsky, P. A.; Ananthapadmanabhan, K. P. Determination of the aggregation number and charge of ionic surfactant micelles from the stepwise thinning of foam films. *Adv. Colloid Interface Sci.* **2012**, *183−184* (0), 55−67.
(62) Evans, D. F.; Allen, M.; Ninham, B. W.; Fouda, A. Critical micelle concentrations for alkyltrimethylammonium bromides in water from 25 to 160 °C. *J. Solution Chem.* **1984**, *13* (2), 87−101.
(63) Evans, D. F.; Chen, S. H.; Schriver, G. W.; Arnett, E. M. Thermodynamics of Solution of Nonpolar Gases in a Fused Salt. "Hydrophobic Bonding" Behavior in a Nonaqueous System. *J. Am. Chem. Soc.* **1981**, *103* (2), 481−482.
(64) Greaves, T. L.; Kennedy, D. F.; Mudie, S. T.; Drummond, C. J. Diversity Observed in the Nanostructure of Protic Ionic Liquids. *J. Phys. Chem. B* **2010**, *114* (31), 10022−10031.
(65) Evans, D. F.; Chen, S. H.; Schriver, G. W.; Arnett, E. M. Thermodynamics of Solution of Nonpolar Gases in a Fused Salt. "Hydrophobic Bonding" Behavior in a Nonaqueous System. *Abstr. Pap.—Am. Chem. Soc.* **1981**, *181* (March), 121-PHYS.
(66) Chu, B.; Wu, G. W.; Schneider, D. K. A Scattering Study on Intermicellar Interactions and Structures of Polymeric Micelles. *J. Polym. Sci., Part B: Polym. Phys.* **1994**, *32* (16), 2605−2614.
(67) Dorshow, R. B.; Bunton, C. A.; Nicoli, D. F. Comparative-Study of Intermicellar Interactions Using Dynamic Light-Scattering. *J. Phys. Chem.* **1983**, *87* (8), 1409−1416.
(68) Greaves, T. L.; Kennedy, D. F.; Weerawardena, A.; Tse, N. M. K.; Kirby, N.; Drummond, C. J. Nanostructured Protic Ionic Liquids Retain Nanoscale Features in Aqueous Solution While Precursor Bronsted Acids and Bases Exhibit Different Behavior. *J. Phys. Chem. B* **2011**, *115* (9), 2055−2066.
(69) Zhang, G. D.; Chen, X.; Zhao, Y. R.; Ma, F. M.; Jing, B.; Qiu, H. Y. Lyotropic liquid-crystalline phases formed by Pluronic P123 in ethylammonium nitrate. *J. Phys. Chem. B* **2008**, *112* (21), 6578−6584.


DOI: 10.1021/jp509557z
*J. Phys. Chem. B* 2015, 119, 179−191